Spatial Characteristics of Wireless Channel in Tunnel with Imperfect Walls

Yi Zhang[1], Zhao Xu[2], Bo-Ming Song[3], Yu Huo*[4]
[1,2,3]School of Information and Electrical Engineering, China University of Mining and Technology, Xuzhou, Jiangsu 221008, China,+86 0516 83884023
[1]Huaibei Mining (Group) Company Ltd., Huaibei, Anhui 235025, China.
[4]The National and Local Joint Engineering Laboratory of Internet Technology on Mine, IOT Perception Mine Research Center, China University of Mining and Technology, Xuzhou, Jiangsu 221008, China.
*Corresponding author, e-mail: huoyu@aliyun.com

Abstract

The successful design and application of the physical layer techniques of the wireless network, including MIMO, adaptive OFDM, and mining antenna, to name a few, need the detailed knowledge of the spatial characteristics of the transmitted signals. This paper provides a modal approach to quantify the spatial distribution of the waves in tunnels in detail. We develop the modal theory for propagation in a tunnel with imperfect walls, which are lossy, rough, and tilted. And then, we discuss the transmission power of the antenna as a function of the angles of departure (AOD). On this basis, we take the half-wave dipole antenna as an example to analyse by simulations. The theoretical results show that the angular power distribution in the rectangular tunnel follows Gaussian distribution. The angle spread (AS) of the waves can be influenced by the tunnel walls. The roughness of the wall surface is most important in small tunnels and at low frequencies, whereas the wall tilt is most important in large tunnels and at high frequencies.

Keywords: modal theory, spatial distribution, tunnel, imperfect walls, wireless network

1. Introduction

Wireless Underground Communication Networks (WUCNs) promise a wide variety of novel applications, such as environmental monitoring, localization, disaster warning in highway and railroad tunnels as well as in underground mines. The main challenge for WUCNs is the realization of efficient and reliable underground wireless links. Physical layer techniques, such as MIMO, adaptive OFDM, and mining antenna, are researched to overcome the severe multipath fading in these special constrained environments [1, 2]. The spatial propagation characteristics in the wireless environment significantly influence the performance of these physical layer techniques, so they should be analysed accordingly [3, 4].

In underground, the tunnel could be viewed as a heavily overmoded waveguide [5-7]. Consequently, the power provided by the antenna can be effectively transmitted only if it is effectively coupled into the allowed propagation modes. Due to the coupling between the antenna and the tunnel waveguide structure and the reflections caused by the tunnel walls, the angular power distribution of the wireless channel is quite different from the terrestrial channel.

Lienard [8] given the map of the directions of arrival at a distance of 40m in a tunnel by measurements and theoretical calculation. It concluded that the spread angle increases with the tunnel size. Zhang [9] measured the received signal power versus the width or the height of the tunnel cross section in two size tunnels. The curves show distorted dominant-mode cosine function. Nasr [10] and Huo [11] calculated the direction of arrival (DOA) in a tunnel by the ray method in straight tunnels. Sun [12] calculated the spatial power distribution of the electromagnetic waves transmission mode in a rectangular tunnel with perfectly conducting walls.

All in all, the related theoretical results been obtained to date are still too limited to guide the design and application of MIMO, adaptive OFDM, and mining antenna, etc. In the practical application, the tunnel walls are rough and may have long range tilt variations. In addition, they

are imperfectly conducting. The influences of these factors on the spatial distribution of the waves were not considered in the above work [8-12].

The goal of this paper is to develop a theoretical analysis to quantify the spatial distribution of the waves in tunnels in detail and to provide a better understanding of the waveguide effects in tunnels. In [4], we have proposed a multimode operating waveguide model. Its emphasis was only on tunnels with small degree tilted walls. In this paper, we extend the work in [6] by considering the case of wall tilt, which the tunnel may also exhibit to a marked degree. The remainder of this paper is organized as follows. In Section 2, we develop the modal theory for propagation in a tunnel with lossy, rough, and tilted walls. We discuss the relationship between the angles of departure (AOD) and the order of each mode in the ray picture. And then on this basis, we get the transmission power as a function of AOD. In Section 3, we evaluate the statistical characteristics of the angular power distribution and the effects of the dielectric properties, roughness and tilt of the tunnel walls.

2. Modal Approach to Angular Distribution of Waves
2.1. The Multimode Model
(1) Straight tunnel model

Here we consider the general case of a radio propagation channel in a rectangular tunnel. Suppose that the rectangular tunnel of w width and h height. Locate the coordinate system in the centre of the tunnel cross section. z axis is defined as the longitudinal direction of the tunnel, x axis as the width, and y axis as the height. Consider K1 is the electrical parameters of the material on the side walls, and K2 corresponding to the roof and floor. The rough surface of the walls is assumed to have a Gaussian distribution with a standard derivation equal to σ_{rough}^2.

In the rectangular waveguide, the electric field E is polarized predominantly in the horizontal and vertical directions, respectively. The main field components are the tangential field components in the tunnel [7]. If the tunnel is straight, for horizontal polarized (m, n) mode, they are [6],

$$\overrightarrow{E_{mn}} \cong \overrightarrow{i_x} \frac{E_{0mn}}{\sqrt{M}} \cos k_{xmn} x \cos k_{ymn} y \rho_{mn} \exp\left(-ik_{zmn} z\right)$$

$$\overrightarrow{H_{mn}} \cong \overrightarrow{i_y} \frac{1}{Z_{mn}} \frac{E_{0mn}}{\sqrt{M}} \cos k_{xmn} x \cos k_{ymn} y \rho_{mn} \exp\left(-ik_{zmn} z\right) \tag{1}$$

Where E_{0mn} is the mode intensity on the excitation plane. We will discuss them later. M is the number of the allowed modes that propagate in the tunnel. Here we define $m = 0,1,2,\cdots,m_{\max}$; $n=0,1,2,\cdots,n_{\max}$; m and n can not equal to 0 at the same time [6],

$$m_{\max} = \frac{2w}{\lambda} \;;\; n_{\max} = \frac{2h}{\lambda} \tag{2}$$

The number of the allowed modes which could propagate in the tunnel M is given by [11, 12]:

$$M = 2\left[(2m_{\max}+1)(2n_{\max}+1)-1\right]$$
$$= \frac{32wh}{\lambda^2} + \frac{8}{\lambda}(w+h) \tag{3}$$

Z_{mn} is the characteristic impedance,

$$Z_{mn} = \frac{E_{mn}}{H_{mn}} = \frac{\omega\mu_0 k_{zmn}}{k_{xmn}^2 + k_{zmn}^2} \tag{4}$$

k_{xmn}, k_{ymn} and k_{zmn} are defined as [7]:

$$k_{xmn} \cong \frac{m\pi}{w} + i\frac{mK1\lambda}{w^2(K1-1)^{1/2}} \tag{5}$$

$$k_{ymn} \cong \frac{n\pi}{h} + i\frac{n\lambda}{h^2(K2-1)^{1/2}} \tag{6}$$

$$k_{zmn} \cong \frac{2\pi}{\lambda} - \frac{i\lambda^2}{2}\left[\frac{m^2 K1}{w^3\sqrt{K1-1}} + \frac{n^2}{h^3\sqrt{K2-1}}\right] \tag{7}$$

$$k_{xmn}^2 + k_{ymn}^2 + k_{zmn}^2 = k_0^2 = \frac{4\pi^2}{\lambda^2} \tag{8}$$

Where λ is the wavelength.

ρ_{mn} is the loss factor caused by the surface roughness [6],

$$\rho_{mn} = \exp\left[-\frac{\pi^2 \sigma_{rough}^2 \lambda z}{2}(\frac{m^3}{w^4} + \frac{n^3}{h^4})\right] \tag{9}$$

(2) Tilted tunnel model

Suppose that there is long range tilt of one vertical wall of the tunnel. Then the ray of a mode encounters a portion of the tilted vertical wall through an angle θ_{tilt1} about the y axis.

Then the electromagnetic field is changed from (1) to:

$$\overline{E_{mn}^{tilt}} \cong \overline{i_x}\frac{E_{0mn}}{\sqrt{M}}\cos k_{xmn}x\cos k_{ymn}y\rho_{mn}\exp\left(-ik_{zmn}\left(z\cos 2\theta_{tilt1} + x\sin 2\theta_{tilt1}\right)\right)$$

$$\overline{H_{mn}^{tilt}} \cong \overline{i_y}\frac{1}{Z_{mn}}\frac{E_{0mn}}{\sqrt{M}}\cos k_{xmn}x\cos k_{ymn}y\rho_{mn}\exp\left(-ik_{zmn}\left(z\cos 2\theta_{tilt1} + x\sin 2\theta_{tilt1}\right)\right) \tag{10}$$

The power coupling factor g_{t1mn} of the disturbed field back into the mode is given by:

$$g_{t1mn} = \frac{\left|\iint E_{mn}\left(E_{mn}^{tilt}\right)^* dxdy\right|^2}{\iint |E_{mn}|^2 \, dxdy \iint \left|E_{mn}^{tilt}\right|^2 dxdy} \tag{11}$$

Then by derivation,

$$g_{t1mn} \cong \exp\left(-\frac{1}{16}k_{zmn}^2 w^2 \sin^2 2\theta_{tilt1}\right) \tag{12}$$

Likewise, if there is long range tilt of one horizontal wall of the tunnel, the ray of a mode encounters a portion of the tilted horizontal wall through an angle θ_{tilt2} about the x axis. Then tilting of the floor or roof gives a coupling factor,

$$g_{t2mn} \cong \exp\left(-\frac{1}{16} k_{zmn}^2 h^2 \sin^2 2\theta_{tilt2} \right)$$

(13)

Suppose that (m, n) mode bounces from wall to wall of the straight tunnel making a grazing angle ϕ_{1mn} with the side walls and ϕ_{2mn} with the floor and roof. Then [6]:

$$\sin\phi_{1mn} = \frac{k_{xmn}}{k_0} \cong \frac{m\lambda}{2w} \;;\; \sin\phi_{2mn} = \frac{k_{ymn}}{k_0} \cong \frac{n\lambda}{2h}$$

(14)

Then in a tilted wall tunnel, the numbers of reflections N_{1mn} and N_{2mn} experienced by a ray at the vertical and horizontal walls of the tunnel, while travelling a distance z along the tunnel, are given by:

$$N_{1mn} \cong \frac{z \sin\phi_{1mn}}{w \cos 2\theta_{tilt1}} \;;\; N_{2mn} \cong \frac{z \sin\phi_{2mn}}{h \cos 2\theta_{tilt2}}$$

(15)

The loss factor for a distance z is:

$$g_{tmn} = \left(g_{t1mn}\right)^{N_{1mn}} \left(g_{t2mn}\right)^{N_{2mn}}$$
$$\cong \exp\left[-\frac{\pi^2 z}{8\lambda} \left(\frac{m \sin^2 2\theta_{tilt1}}{\cos 2\theta_{tilt1}} + \frac{n \sin^2 2\theta_{tilt2}}{\cos 2\theta_{tilt2}} \right) \right]$$

(16)

Then field strength in a tilted tunnel can be expressed by the approximating function.

$$E_{mn} \cong \frac{E_{0mn}}{\sqrt{M}} \cos k_{xmn} x \cos k_{ymn} y \rho_{mn} \sqrt{g_{mn}} \, \mathrm{Re}\left[\exp\left(-ik_{zmn} z\right) \right]$$
$$H_{mn} \cong \frac{1}{Z_{mn}} \frac{E_{0mn}}{\sqrt{M}} \cos k_{xmn} x \cos k_{ymn} y \rho_{mn} \sqrt{g_{mn}} \, \mathrm{Re}\left[\exp\left(-ik_{zmn} z\right) \right]$$

(17)

2.2. Power Distribution Versus AOD

Define the excitation plain at z=0. Assuming a horizontally polarized transmitting antenna that is located at (x0, y0, 0) in the tunnel. Its surface current distribution is $\overline{K}$.

According to (1), by matching the tangential boundary conditions over the cross section containing the antenna, for (m, n) mode we obtain:

$$E_{0mn} = -\frac{Z_{mn}}{2\sqrt{M}} \cdot$$
$$\iiint_v \left(\vec{i}_z \times \overline{K}\right) \Box \left(\vec{i}_y \cos\left(k_{xmn} x\right) \cos\left(k_{ymn} y\right) \exp\left[-ik_{zmn}\left(z - z0\right)\right]\right) dV$$

(18)

For one direction of the tunnel, the left or the right of the antenna, the transmission power of the (m, n) mode is:

$$P_{mn} = \frac{1}{2} \iint_{x,y} \frac{E_{mn}^2}{Z_{mn}} = wh \frac{E_{mn}^2}{2Z_{mn}}$$

(19)

Here we characterize AOD of (m, n) mode in the ray picture by the azimuth angle φ_{mn} and elevation angle θ_{mn}. φ_{mn} is the angle between the projection of the ray at the horizontal

plane and x axis. Its boundary is $[0, 2\pi]$. θ_{mn} is the angle between the ray and y axis. Its boundary is $[0, \pi]$. Figure 1 shows the spatial parameters of a mode in the ray picture. They are [11, 13]:

$$\varphi_{mn} \cong \delta_{\varphi}\pi + \frac{\pi}{2} \pm \arcsin(\frac{m\lambda h}{w\sqrt{4h^2 - n^2\lambda^2}}) ; \ \theta_{mn} \cong \frac{\pi}{2} \pm \arcsin(\frac{n\lambda}{2h}) \tag{20}$$

When the receiving antenna is in the front of the transmitting antenna, $\delta_{\varphi} = 0$, otherwise, $\delta_{\varphi} = 1$.

Then we can get the relationships between m, n and AOD:

$$m = \frac{2w}{\lambda}\sin\theta\cos\varphi ; \ n = \frac{2h}{\lambda}\cos\theta \tag{21}$$
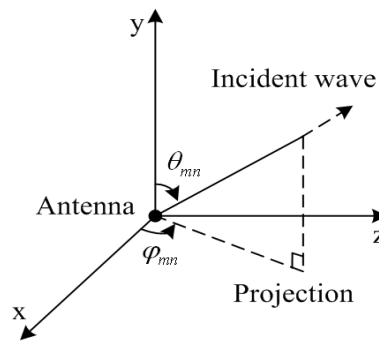
Figure 1. Azimuth Angle and Elevation Angle of a Wave in Coordinal System

On combining (2)-(9), (16)-(19) and (21), we could obtain the transmission power $p(\theta, \varphi)$ of a horizontally polarized antenna described by AOD. The transmission power of a vertically polarized antenna can be obtained by the same way.

3. Results and Discussion

In this section, we begin with an initial example that illustrates the spatial distribution of the power in a rectangular tunnel. Then we analyze the effects of various tunnel conditions.

Except studying the effects of certain parameters, the default tunnel conditions are set as follows: the tunnel cross section shape is a rectangle with a height of 4m and a width of 6 m; consider the general case that the walls of the tunnel are made of the same material with electrical parameters K1=K2=10-j0.18; the carrier frequency is set to 900MHz; the rough surface has a Gaussian distribution with a standard derivation equal to 0.08m; the side wall is tilted through 1° about the vertical axis.

In this paper we take a horizontally polarized half-wave dipole, which is the most typical linear antenna and easy to transform into many other antennas, as an example to analyse.

Then the surface current distribution of the transmitting antenna is:

$$\overline{K} \cong \overline{i}_x I_0 \cos\left(\frac{2\pi x}{\lambda}\right)\delta(y - y_0)\left[u\left(x - \left(x_0 - \frac{\lambda}{4}\right)\right) - u\left(x - \left(x_0 + \frac{\lambda}{4}\right)\right)\right] \tag{22}$$

It is located in the middle of the tunnel cross section. The observation point is 100m away from the transmitter and in the middle of the tunnel cross section.

3.1. Angular Power Distribution

[11] computed the angular power distribution in a rectangular tunnel with perfect walls, which is straight and smooth. It concluded that the distribution follows Gaussian distribution. In this paper, we analyse the distribution in a tunnel with imperfect walls, which is lossy, rough and tilted. Figure 2(a) presents the transmission power versus AOD deduced from the modal approach. We normalize the power of each mode by the maximum power among modes. Gaussian distribution defined in [14] and Laplacian distribution defined in [15] are two typical angular power distributions for terrestrial environments. We compare their power angle profile in Figure 2(b) and (c). To generate graphs of these 2 probability density functions, the values of the mean path AOD φ_0, θ_0 and the angle spread (AS) σ_φ, σ_θ have been calculated so that they deduced either from the Gaussian distribution or from the actual distribution of the field are identical. They are given by:

$$\varphi_0 = E\{\varphi\} \; ; \; \theta_0 = E\{\theta\} \tag{23}$$

$$\sigma_\varphi = \sqrt{E\{\varphi^2\} - \left[E\{\varphi\}\right]^2} \; ; \; \sigma_\theta = \sqrt{E\{\theta^2\} - \left[E\{\theta\}\right]^2} \tag{24}$$

By comparison, we get a good agreement between graphs in Figure 2 (a) and (b), whereas there is a significant difference between figures in Figure 2(a) and (c). It can be concluded that AOD distribution in the rectangular tunnel still follows Gaussian distribution, even consider the roughness and tilt of the walls.

(a) Theoretical distribution

(b) Gaussian distribution

(c) Laplacian Distribution
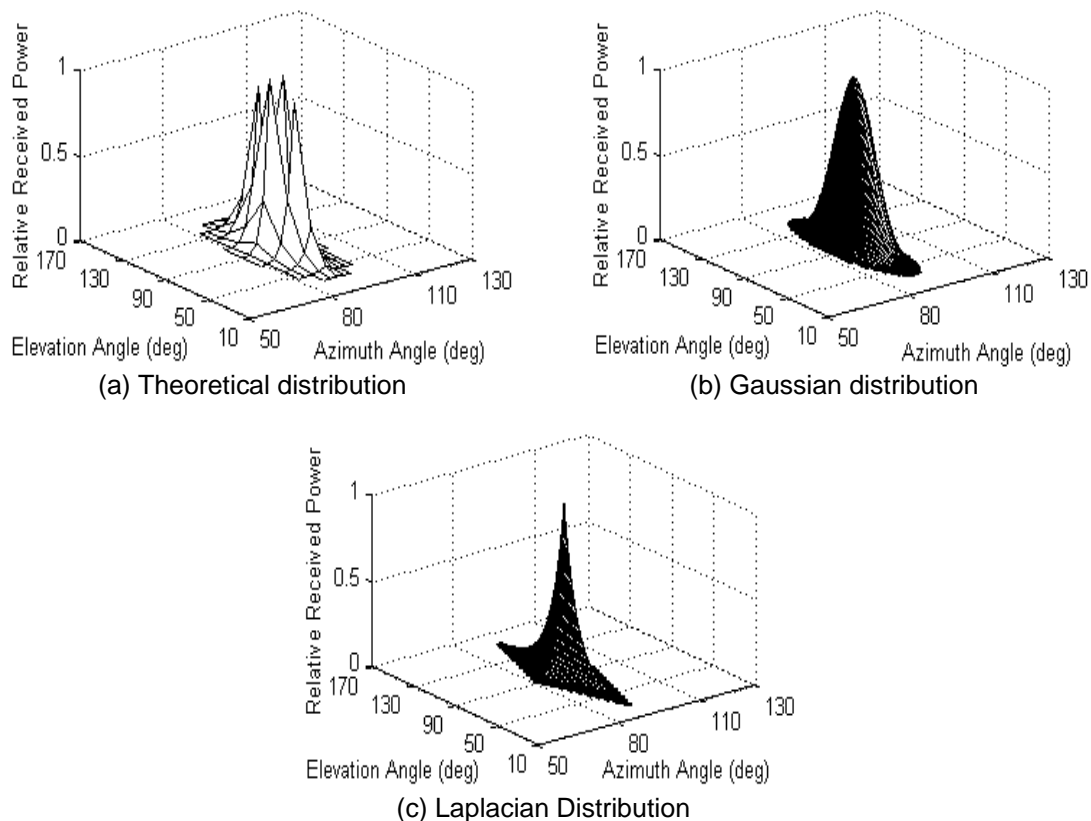
Figure 2. Radiation Field Distribution

3.2. Effects of Lossy Walls

The electrical parameters of the material on the walls K1 and K2 are defined as [14]:

$K_1 = \varepsilon_1 - j\dfrac{\sigma_1}{2\pi f \varepsilon_0}; K_2 = \varepsilon_2 - j\dfrac{\sigma_2}{2\pi f \varepsilon_0}$, where $\varepsilon_0 = 8.85 \times 10^{-12}$ F/m is the permittivity in

vacuum space. ε_1 and ε_2 are the relative permittivity for the side walls or roof and floor in the tunnel; σ_1 and σ_2 are their conductivity. They are influenced by the humidity, pressure and temperature of the surrounding rock. Look up in [16-19], ε_1 and ε_2 are in the range of 2~70; σ_1 and σ_2 are in the range of 10-6~1S/m. On substituting into K1 and K2, we can find that the effect of conductivity could be completely negligible due to the small value compared to the permittivity. In Figure 3 we give the curves of AS versus the relative permittivity. Suppose that $\varepsilon_1 = \varepsilon_2$ and $\sigma_1 = \sigma_2 = 0.009\text{S/m}$. It is shown that the influence of the relative permittivity is greater when its value is small, around 2-10.
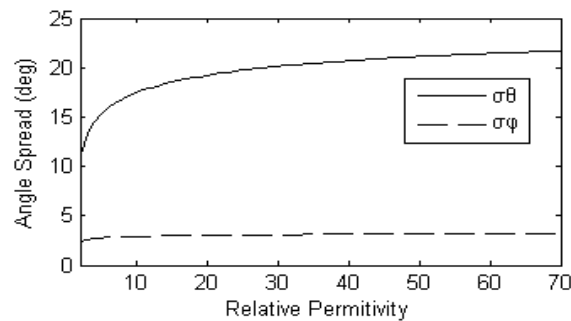
Figure 3. Angle Spread Versus Relative Permittivity

3.3. Effects of Rough and Tilted Walls

To analyze the effects of the wall roughness and wall tilt on the spatial distribution of the waves, we compare 3 tunnel conditions in this part: smooth walls and straight tunnel, rough walls and straight tunnel, rough walls and one side wall is tilted.

The wall roughness and wall tilt could influence the transmission power distribution in each direction by the tunnel size and the operating frequency [1, 7].

At first, we analyze the variation of AS with the tunnel size for the above 3 tunnel environments. We calculate AS with different width in a tunnel of 4 m height In Figure 4(a) and AS with different height in a tunnel of 4m width in Figure 4(b).

It is shown that for straight tunnels, AS increases with the size of the tunnel. This result coheres with that obtained by ray method in [11] and by measurements in [8]. Firstly, in a ray picture of a given mode, the grazing angles of the ray decrease with the size of the tunnel cross section [1, 7]. This results in a decrease of the spread of angle of the ray relative to the direct path. Secondly, both of the loss owing to reflection and scattering by the walls and the number of bounces per unit length decrease for the grazing angles. It results that the transmission power increases. Thirdly, the large the tunnel size, the more the number of propagation modes [6]. Consequently, increase in tunnel transverse dimensions decreases the first factor but increases the last two factors. Then the net effect is an increase of AS with the tunnel size.

While for the third condition that there is long range tilt of the tunnel walls, we can see in Figure 4(a) that σ_θ decreases with the width, and in Figure 4(b) that σ_φ and the percentage increase of σ_θ decrease with the height. The reason is that, the reflected mode will be rotated into other mode when the tunnel exhibits to a marked degree tilt. From (13)–(16), the corresponding order of the mode is higher for a given direction in the larger tunnel. Then the power of the disturbed field coupled back into the wave is smaller in the larger tunnel for a given

propagation distance. This results in larger scattering loss in the larger titled tunnel. Consequently, the wall tilt contributes to the decrease of AS with the tunnel size. And the larger the tunnel, the more roles the wall tilt plays.

To sum up, the roughness is more important in small tunnels while tilt is more important in large tunnels.

(a) Angle spread versus width of the tunnel   (b) Angle spread versus height of the tunnel
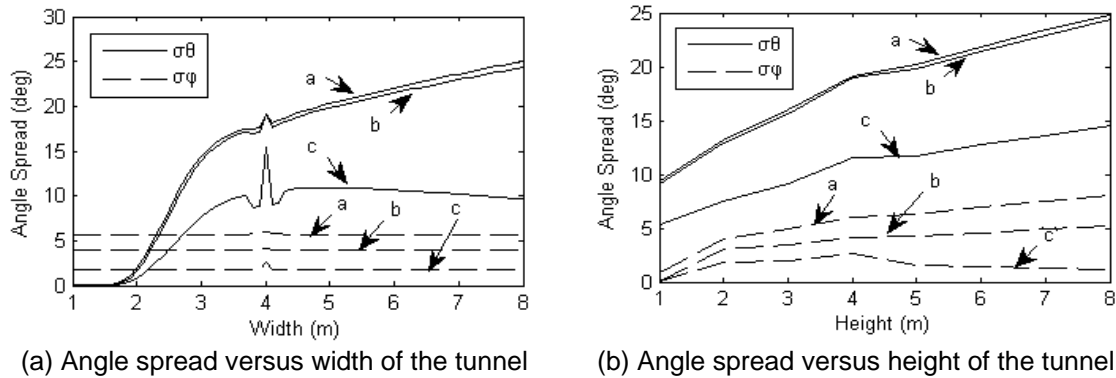
Figure 4. Angle spread versus size of tunnel cross section. Case (a) $\sigma^2_{rough} = 0m, \theta_{tilt} = 0°$; Case (b) $\sigma^2_{rough} = 0.08m, \theta_{tilt} = 0°$; Case c. $\sigma^2_{rough} = 0.08m, \theta_{tilt} = 1°$

Secondly, we analyze the variation of AS with the operating frequency for the above 3 tunnel environments.

In Figure 5 we illustrate the effects of operating frequency on σ_φ and σ_θ. The above 3 tunnel conditions are considered. It is shown that for the straight tunnels, AS varies directly with the frequency, especially when it is lower than 500MHz. This result coheres with that obtained by ray method in [11]. But for the tunnel with tilted walls, the AS decreases with the frequency at high frequencies.

Increase in frequency decreases the grazing angles defined by each mode and increases the propagation modes number. Then the mechanism that the effect of frequency on AS is similar to the mechanism that the effect of tunnel size on AS. Besides, from (9) and (16), it is also shown that the roughness is more important at low frequencies while the wall tilt is more important at high frequencies.
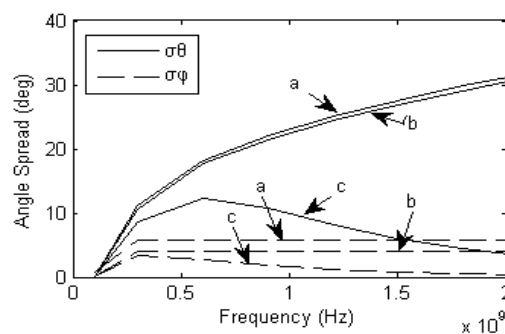
Figure 5. Angle Spread Versus Carrier Frequency. Case (a) $\sigma^2_{rough} = 0m, \theta_{tilt} = 0°$; Case (b) $\sigma^2_{rough} = 0.08m, \theta_{tilt} = 0°$; Case c. $\sigma^2_{rough} = 0.08m, \theta_{tilt} = 1°$

4. Conclusion

The statistical characteristics of the radiation field distribution of a half-wave dipole antenna in the rectangular tunnel are discussed by modal approach. The analysis shows that:

(1) The spatial distribution of the waves in the rectangular tunnels follows Gaussian distribution regardless of whether the tunnel walls are rough and tilted.

(2) Angle spread in tunnels could be affected by the humidity, pressure and temperature of the tunnel walls. The effect of conductivity could be negligible, but the contribution of the relative permittivity of the material can not, especially when its value is low.

(3) The roughness of the wall surface is most important in small tunnels and at low frequencies. It will cause that AS increases with the tunnel size and the operating frequency. The wall tilt is most important in large tunnels and at high frequencies. It will cause that AS decreases with the tunnel size and the operating frequency.

Acknowledgements

References

[1] Guan K, Zhong ZD, et al. Measurement of distributed antenna systems at 2.4GHz in a realistic subway tunnel environment. *IEEE Transactions on Vehicular Technology*. 2012; 61(2): 834-837.
[2] Akyildiz IF, Sun Z, Vuran MC. Signal propagation techniques for wireless underground communication networks. *Physical Communication*. 2009; 2(3): 167–183.
[3] Zhang LW. Sparsity-based Angle of Arrival Estimation for Emitter Localization. *TELKOMNIKA Telecommunication Computing Electronics and Control*. 2012; 10(4): 769-774.
[4] GUO LM, Nian XH. Time of Arrival and Angle of Arrival Statistics for Distant Circular Scattering Model. *TELKOMNIKA Telecommunication Computing Electronics and Control*. 2012; 10(3): 564-571.
[5] Pao HY. Probability Density Function for Waves Propagating in a Straight PEC Rough Wall Tunnel. *Microwave and Optical Technology Letters*. 2005; 44(5): 427-430.
[6] Huo Y, Xu Z, Zheng HD. Characteristics of multimode propagation in rectangular tunnels. *Chinese Jounal of Radio Science*. 2010; 25(6): 1225-1230.
[7] Emslie AG, Lagace RL, Strong PF. Theory of the propagation of UHF radio waves in coal mine tunnels. *IEEE Trans. Antennas and Propagation*. 1975; AP-23(2): 192-205.
[8] Lienard M, Degauque P. Natural wave propagation in mine environments. *IEEE Trans. Antenna Propag*. 2000; 48(9): 1326-1339.
[9] Zhang YP, Hwang Y. Characterization of UHF radio propagation channels in tunnel environments for microcellular and personal communications. *IEEE Trans. Veh. Technol*. 1998; 47(1): 283-296.
[10] Nasr A, Molina JM, Lienard M, et al. *Optimisation of Antenna Arrays for Communication in Tunnels*. In ISWCS for wireless communication systems. Valencia. 2006. 522-524.
[11] Huo Y, Wang TT, Liu FX, Xu Z. Angular power distribution of wireless channel in mine tunnel. *TELKOMNIKA*. 2013; 11(3): 1422-1435.
[12] Sun JP, Gao MF. Research on the radiation characteristics of symmetrical dipole antenna in rectangular tunnel. *Journal of China Coal Society*. 2010; 35(12): 2121-2124.
[13] Huo Y, Xu Z, Liu FX. A Wave Propagation Model Combined the Modal Theory and Ray Theory in Coal Mine Tunnels. *ACTA Electronica Sinica*. 2013; 41(1): 110-116.
[14] Adachi F, Feeney M, Williamson A, Parsons J. Cross correlation between the envelopes of 900MHz signals received at a mobile radio base station site. *Iet Software*. 1986; 133(6): 506-512.
[15] Pedersen KI, Mogensen PE, Fleury BH. Power azimuth spectrum in outdoor environments. *Electron Lett*. 1997; 33(18): 1583-1584.
[16] LEE WCY. Effects on correlation between two mobile radio base-station antennas. *IEEE Trans. Veh. Technol*. 1973; 22(4): 1214-1224.
[17] Xu HW. Measurement and test of seam electric parameter and study on relationship between seam electric parameter and coal petrology characteristics. *Coal Science and Technology*. 2005; 33(3): 42-47.
[18] Cheng LF, Sun JP. Influence of electrical parameters on electromagnetic waves propagation in rectangular tunnels. *Chinese Journal of Radio Science*. 2007; 22(3): 513-517.
[19] Luo JA, Wang LG, Tang FR, He Y, Zheng L. Variation in the temperature field of rocks overlying a high-temperature cavity during underground coal gasification. *Mining Science and Technology (China)*. 2011; 21(5): 709-713.